Reac Kinet Mech Cat (2016) 119:555–568
DOI 10.1007/s11144-016-1061-2

Liquid phase hydrogenation of adiponitrile over acid-activated sepiolite supported K–La–Ni trimetallic catalysts

Yang Lv[1,2] · Fang Hao[1] · Pingle Liu[1,2] · Shaofeng Xiong[1] · Hean Luo[1,2]

Received: 16 May 2016 / Accepted: 28 July 2016 / Published online: 18 August 2016

Abstract Acid-activated sepiolite (ASEP) supported K–La–Ni trimetallic catalysts were prepared and tested in the liquid phase hydrogenation of adiponitrile (ADN). The sepiolite was treated with dilute hydrochloric acid solution to obtain ASEP, ASEP supported K–La–Ni trimetallic catalysts were prepared by the incipient impregnation method and characterized by nitrogen adsorption–desorption, temperature programmed reduction, hydrogen chemisorption, powder X-ray diffraction, transmission electron microscopy, scanning electron microscopy, Fourier transform infrared spectroscopy and energy dispersive X-ray. It was revealed that potassium could inhibit the formation of the 1-azacycloheptane by-product by neutralizing some acid sites on the catalyst, and the potassium and lanthanum could efficiently reduce nickel particles size and improve its dispersion. Sepiolite treated with hydrochloric acid increases the number of silanol groups (Si–OH) on the sepiolite surface, which is helpful to nickel particles adsorption and dispersion. ASEP supported K–La–Ni trimetallic catalysts (K–La–Ni/ASEP) present better catalytic performance under mild reaction conditions of 373 K and 2.0 MPa, the ADN conversion reaches to 90.03 %, the selectivity to 6-aminocapronitrile and hexamethylenediamine is up to 90.22 %.

Electronic supplementary material The online version of this article (doi:10.1007/s11144-016-1061-2) contains supplementary material, which is available to authorized users.

✉ Fang Hao
haofang.happy@163.com

✉ Pingle Liu
liupingle@xtu.edu.cn

[1] College of Chemical Engineering, Xiangtan University, Xiangtan 411105, China

[2] National & Local United Engineering Research Centre for Chemical Process Simulation and Intensification, Xiangtan University, Xiangtan, China

Keywords Adiponitrile · Hydrogenation · 6-Aminocapronitrile · Hexamethylenediamine · Acid-activated sepiolite · K–La–Ni trimetallic catalysts

Introduction

The catalytic hydrogenation of nitriles is an important industrial route for the manufacture of a great variety of amines, and the nitrile hydrogenation products are mainly composed of a mixture of primary, secondary and tertiary amines [1–3]. Condensation reactions can appear when the highly reactive intermediate imine reacts with the primary amine [4, 5]. The typical instance of these is the hydrogenation of adiponitrile (ADN) to 6-aminocapronitrile (ACN), which is an interesting industrial process in the preparation of ε-caprolactam (precursor of Nylon-6) and hexamthylenediamine (HMDA), which is used in the preparation of Nylon-66 [6–9]. The traditional technology for ε-caprolactam production mainly uses aromatic hydrocarbon as materials under multi-step processes and result in large amount of ammonium sulfate by-product [6]. Recently, researchers have paid much attention to new methods for ε-caprolactam production with lower cost and environmental pollution. Compared with the traditional production method for ε-caprolactam, the route of butadiene hydrocyanation is one of green production processes with many advantages. The process includes the butadiene hydrocyanation to ADN, the hydrogenation of ADN to ACN and the cyclization of ACN in the presence of water to prepare ε-caprolactam [7–9]. Among these steps, ADN selective hydrogenation to ACN is the key step, and its deep hydrogenation products are HMDA and Schiff bases [9].

ADN hydrogenation can be carried out in gas or liquid phase [10–15]. Hexing Li et al. [16, 17] have prepared a series of nickel-based amorphous catalysts (Ni–P and Ni–B) for the gas phase hydrogenation of ADN under elevated temperature and high space velocity, the main product is HMDA and the selectivity of ACN is only 32 % at the conversion of 78 %. Sara et al. [10, 11, 13] reported the application of Ni–MgO catalyst in ADN hydrogenation, the ADN conversion is 87 % and the selectivity to ACN is 83 %. Medina et al. [18–22] investigated a series of Fe–Ni catalysts and alumina-supported nickel catalysts in gas phase hydrogenation of ADN and the ACN yield could be up to 85 %. Recently, Raney Ni or Co has been widely used in liquid phase hydrogenation of ADN under high hydrogen pressure in ammonia or alkali metal hydroxide solution [23–28]. However, besides the shortcomings of Raney catalysts, it needs a large amount of ammonia to inhibit the formation of secondary and tertiary amines. It has been reported that the selective hydrogenation of ADN to primary amine is structure sensitive. Therefore, the selectivity to ACN and HMDA could be significantly improved by modifying the surface of the catalyst so as to reduce the generation active sites for 1-azacycloheptane (ACH). It has been shown that the specific activity of the nickel catalysts strongly depend on the promoters and the type of the supported metal [14, 15, 18, 22, 29].

Sepiolite has a fibrous structure and an open porous network. It can be used as catalytic support due to its peculiar structure [30, 31]. Acid treatment of sepiolite can remove the brucitic magnesium octahedral layers, and the sepiolite will transform into amorphous fibrous silica and generate enough octahedral vacancies,

which are easy to incorporate with different mental cations. Sepiolite has high absorbing capacity due to its peculiar pore structure. Silanol groups are developed by acidic hydrolysis reactions leading to an increase in both surface area and pore volume and these surface silanol groups (Si–OH) are the main active centers for adsorption [32–34]. The modified sepiolite used as catalyst has been studied with addition of Cu, Fe, Co, and Ni [35].

In this work, hydrochloric acid activated sepiolite was used as support for loading nickel, potassium and lanthanum. The prepared K–La–Ni trimetallic catalysts were tested in liquid phase of ADN hydrogenation under lower temperature. It shows high activity and selectivity to ACN and HMDA.

Experimental

Materials

Adiponitrile (ADN) (98.5 wt%), 6-aminocapronitrile (ACN) (98 wt%) and hexamethylenediamine (HMDA) (99 wt%) were purchased from J&K scientific LTD. Sepiolite was purchased from Henan Xinglei Sepiolite Limited Company, (chemical composition: 42.21 % SiO_2, 20.57 % MgO, 18.83 % CaO, 0.37 % Al_2O_3, 0.21 % Fe_2O_3, 0.18 % K_2O, 0.08 % Na_2O, 0.05 % MnO, 0.02 % P_2O_5, 0.017 % TiO_2, 0.012 % FeO and 15.57 % lost on ignition). The analytical grade of Hydrogen peroxide (30 wt%), $Ni(NO_3)_2.6H_2O$, KNO_3, $La(NO_3)\cdot 6H_2O$ and ethanol were purchased from Sinopharm Chemical Reagent Corporation Limited. H_2 (99.99 %) was purchased from Zhuzhou Diamond Gas Company.

Catalyst preparation

Sepiolite (SEP) was purified and micronized by a wet process. Then the SEP powder was washed by deionized water and treated with hydrochloric acid with the solid-to-liquid ratio of 1:15 at 348 K under mechanical agitation for 24 h. The mixture was filtered, and the precipitate was washed with distilled water and dried at 393 K for 3 h. The SEP treated with hydrochloric acid was labeled as ASEP. During the acid treatment, it can be seen from Scheme 1 (in Supplementary Material) that the Si–O–Mg–O–Si bond in SEP turns into two Si–OH bonds [36].

The catalysts were prepared by the incipient impregnation method. The pretreated SEP was firstly impregnated in the solution of $Ni(NO_3)_2\cdot 6H_2O$, KNO_3 and $La(NO_3)\cdot 6H_2O$ at 303 K for 10 h, and then the samples were dried at 393 K in air for 12 h, calcined under flowing N_2 at 623 K for 4 h and reduced in flowing H_2 at 673 K for 4 h. The prepared catalysts were denoted as Ni/SEP, K–La–Ni/SEP, Ni/ASEP and K–La–Ni/ASEP, respectively. The loading content of nickel is 20 wt%, the content of the potassium is 0.5 wt% and the content of the lanthanum is 2.0 wt%, respectively.

Catalyst characterization

Quantachrome NOVA-2200e automated gas sorption system was used to characterize the specific surface area, pore volume and pore size distribution by the nitrogen adsorption–desorption. The specific surface area of the samples was calculated according to the Brunauer–Emmett–Teller (BET). The pore volume and pore size distributions were analyzed using Barrett–Joyner–Halenda (BJH) methods.

Powder X-ray diffraction (XRD) analysis of the samples was determined using a D/max 2500 TC diffractometer equipped with a back monochromator operating. The tube voltage was 40 kV and a tube current of 30 mA using Cu K_α radiation ($\lambda = 1.542$ Å). The 2θ angle that range from 5° to 90° with a scanning rate of 1° min^{-1}.

Fourier transform infrared spectroscopy (FTIR) was obtained by using a Shimadzu IR Prestige-21 spectrometer.

Energy dispersive X-ray (EDX) elementary mappings were obtained with an FEI Tecnai G^2F30 S-TWIN field emission transmission electron microscope equipped with an EDX spectrometer operating at 300 kV.

Temperature programmed reduction (TPR) was carried out in a Quantachrome ChemBET-3000 instrument, equipped with a 273–1273 K procedure temperature-controlled furnace and a thermal conductivity detector (TCD). Each sample was first heated to 473 K in an argon flow for 2 h. Then, the sample was heated from 473 to 1173 K at a rate of 5 K min^{-1} under 40 mL min^{-1} 5 vol% of H_2/Ar flow.

Hydrogen chemisorption was also measured on a ChemBET 3000 instrument equipped with a procedure temperature-controlled furnace and a thermal conductivity detector (TCD). The sample had been previously reduced at 523 K for 12 h in hydrogen stream, and then the adsorbed hydrogen on the nickel surface was removed under flowing argon stream. The sample was subsequently cooled to ambient temperature under the argon stream. The hydrogen pulses (0.02 mL) were injected until the eluted areas of consecutive pulses became constant. The nickel surface area was calculated by assuming the stoichiometry of one hydrogen molecule per two surface nickel atoms and an atomic cross-sectional area of a nickel atom of 6.49×10^{-20} m^2/Ni atom.

The scanning electron microscope (SEM) images were obtained by using a JEOL JSM-6610LV scanning microscope operating at an accelerating voltage of 5 kV.

The samples were observed by transmission electron microscopy (TEM) conducted on a JEOL 2010 FEG microscope at 200 kV. Each sample was prepared by dispensing a small amount of dry powder in ultrapure water. Then, the suspension was dropped on 300 mesh copper TEM grids covered with thin amorphous carbon films. The instrumental magnification ranged from 2×10^4 to 10×10^6.

Procedure for the catalytic test

The liquid phase hydrogenation of ADN was carried out in a 100 mL Teflon-lined stainless steel autoclave equipped with temperature detector, pressure controller and magnetic stirrer. Generally, 1 g of catalyst, 50 mL of ethanol and 5 g of ADN were

added into the autoclave. The reactor was sealed and purged with H_2 to exclude air, and then it was pressurized to 2 MPa with H_2 under vigorous stirring when it was heated to the setting temperature. After reaction, the catalyst was separated by filtration, and then the contents of the reactants (ADN) and the products (ACN and HMDA) were determined by GC (GC-14C, SHIMADZU) with a flame ionization detector (FID) and a 30 m DB-1701 capillary column using dimethyl phthalate (DMP) as the internal standard. The conversion of ADN and the selectivity to ACN and HMDA were calculated as:

$$\text{ADN conversion} = \frac{\text{Moles of converted ADN}}{\text{Moles of ADN feedstock}} \times 100\,\% \quad (1)$$

$$\text{ACN selectivity} = \frac{\text{Moles of ACN}}{\text{Moles of converted ADN}} \times 100\,\% \quad (2)$$

$$\text{HMDA selectivity} = \frac{\text{Moles of HMDA}}{\text{Moles of converted ADN}} \times 100\,\% \quad (3)$$

Results and discussion

Characterization of catalysts

The textural properties are summarized in Table 1. It can be seen from Table 1 that the surface area of ASEP is larger than that of the original sepiolite. Since acid treatment can open up the SEP internal closed cells, remove a portion of the impurities and increase the porosity, the internal bare fibers increase and the specific surface area increases as well. Moreover, it can be seen from Table 1 that the surface areas decreases when the metals are introduced into the support. Furthermore, it has been reported that the La^{3+} cannot diffuse into the micropore channels of the needle-shaped silicate particles of the support because of its large ion diameter [37]. It suggests that there are some lanthanum oxides on the surface of the support, which leads to the decrement of the BET surface areas. It can be seen

Table 1 Textural property of different catalysts

Catalysts	BET surface area ($m^2\ g^{-1}$)	Average pore diameter (nm)	Pore volume ($cm^3\ g^{-1}$)
SEP	28.3	6.0	0.03
ASEP	124.7	5.9	0.13
Ni/SEP[b]	17.3	13.2	0.06
K–La–Ni/SEP[a,b]	8.6	21.6	0.06
Ni/ASEP[b]	40.2	11.4	0.09
K–La–Ni/ASEP[a,b]	28.7	14.0	0.09

[a] The K/Ni mass ratio = 2.5 % and La/Ni mass ratio = 10 %

[b] The reduction temperature of the catalysts was 673 K

from Table 1 that lanthanum promoted catalyst such as K–La–Ni/SEP and K–La–Ni/ASEP present relatively smaller BET surface areas.

Fig. 1 shows the nitrogen adsorption–desorption curves and BJH pore size distributions of different samples. All the isotherms are of type IV according to the IUPAC classification, representing capillary condensation of nitrogen within the mesoporous structure. All the hysteresis loops are of type H4, which is associated with slit-shaped pores resulting from cumulating of layer structures. According to the geometric effect and Kelvin equation, larger area of the hysteresis loop indicates more pores, which is in good agreement with the pore volume data in Table 1.

The morphology and microstructure of the samples are shown in Fig. 1-S. It is worthy to note that the original fibrous morphology of SEP is kept after acid treatment. Fig. 1-Sa shows that SEP has a stick-like aggregation made up of lots of fibers. It can be seen from Fig. 1-Sb, that the majority of those fibers were cleaved after acid treatment. Fig. 1-Sc and Sd indicates that nickel, potassium and lanthanum particles cover on the surface of the support, which lead to the decrement of the surface areas of the catalysts.

Fig. 2 illustrates the FT-IR spectra of SEP and ASEP. The bands at 3437 cm^{-1} correspond to stretching vibrations of silanol groups (Si–OH) in the octahedral sheet [38]. The bands around 1021 cm^{-1}, which are attributed to Si–O–Si stretching, still

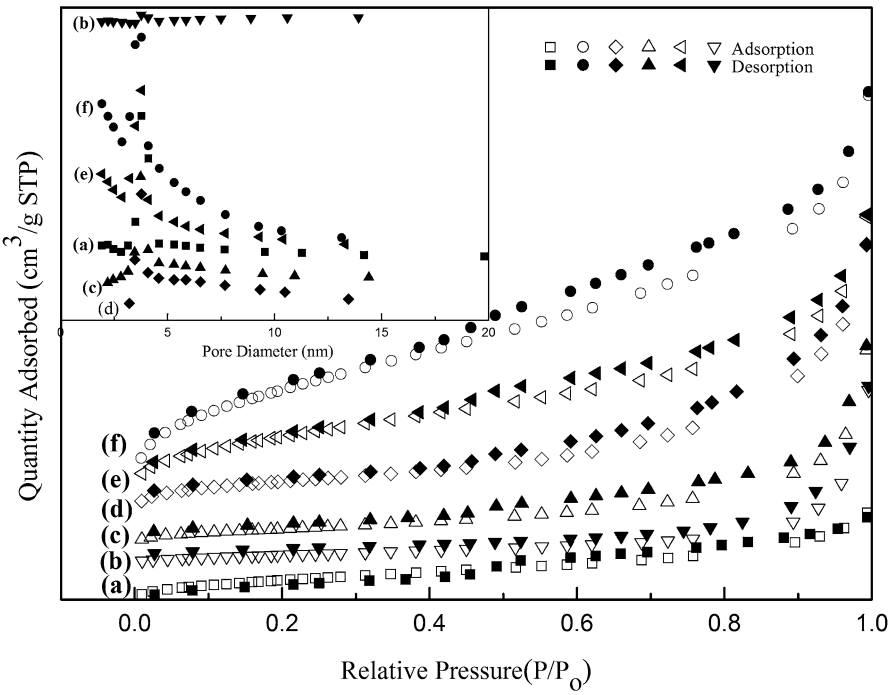

Fig. 1 N_2 adsorption–desorption isotherms and BJH pore size distributions of different samples. SEP (*a*), K–La–Ni/SEP (*b*), Ni/SEP (*c*), Ni/ASEP (*d*), K–La–Ni/ASEP (*e*) and ASEP (*f*). The reduction temperature of the catalysts was 673 K. The K/Ni mass ratio = 2.5 % and La/Ni mass ratio = 10 %

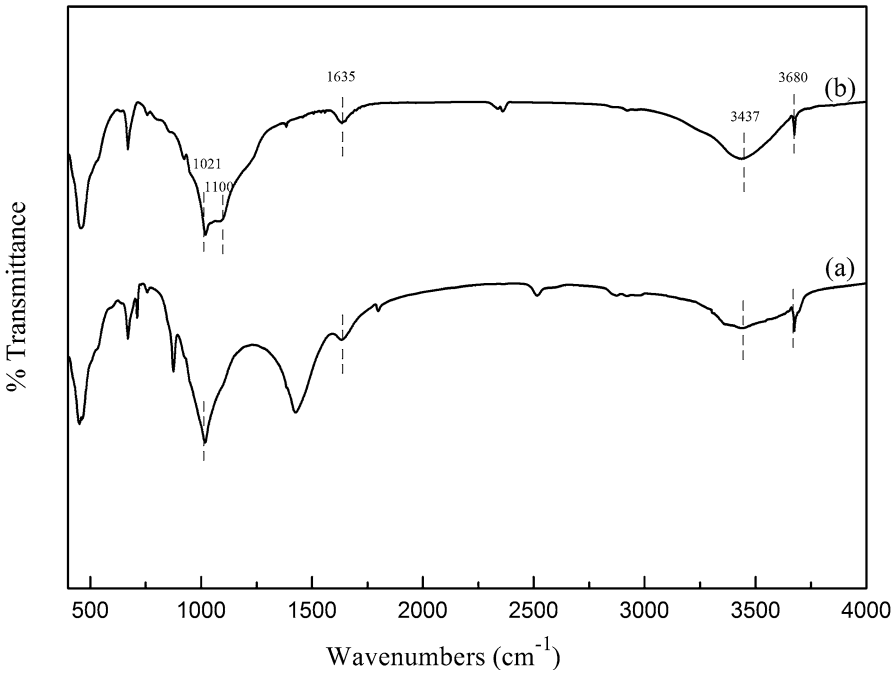

Fig. 2 FT-TR spectra of SEP (*a*), ASEP (*b*)

exist in ASEP [39], which means that the basic structure of sepiolite is not destroyed. The Si–O–Si vibration band at 1100 cm^{-1} appear obvious shoulder peak in ASEP [40], indicating that the bond angle of Si–O–Si band in tetrahedral sheet is changed. The reason may be that the Mg in the lattice is replaced by H^+. The intensity of the band at 3680 cm^{-1} decreases due to the bending vibration of Mg–OH, indicating that Mg is extrated from the lattice and replaced by H^+ during the acid activation process. The band around 1635 cm^{-1} is ascribed to the bending vibration of –OH bond of zeolitic water [41]. The bands at 3437 and 1635 cm^{-1} are progressively broadened in ASEP, it suggests that considerable proportion of silanol groups form after hydrochloric acid treatment.

The TPR profiles of the unreduced samples are shown in Fig. 3. The TPR curves show that the different catalyst precursors have different initial reduction temperature, and the optimal reduction temperature is around 673 K. Compared with the precursor of NiO/ASEP, the TPR peaks of La_2O_3–NiO/ASEP and K_2O–La_2O_3–NiO/ASEP are significantly shifted toward lower temperature when lanthanum is introduced, it may be the electronic transfer due to the strong interaction between NiO and La_2O_3 and this promote the reduction of NiO [37]. The hydrogen consumption peak of NiO/SEP is wider than K_2O–La_2O_3–NiO/SEP, the reason may be that the reduction rate of NiO/SEP decreases because of the interaction between K_2O and NiO. Moreover, the peaks are shifted toward lower temperature when the SEP is treated with hydrochloric acid. The order of the initial reduction temperature of the samples are NiO/SEP > NiO/ASEP. The number of

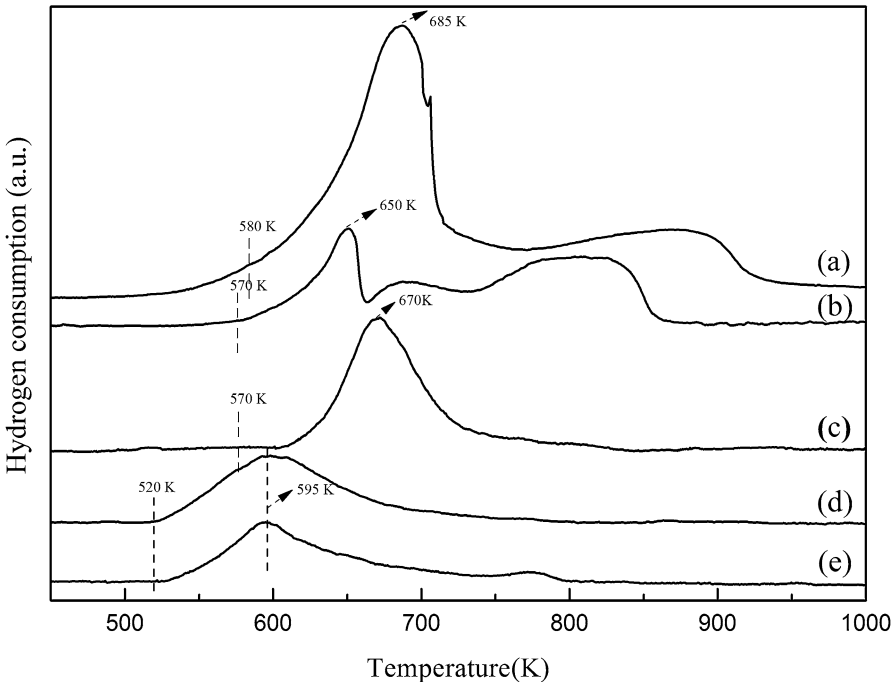

Fig. 3 H_2-TPR profiles of NiO/SEP (*a*), K_2O–La_2O_3–NiO/SEP (*b*), NiO/ASEP (*c*), La_2O_3–NiO/ASEP (*d*), K_2O–La_2O_3–NiO/ASEP (*e*). The K/Ni mass ratio = 2.5 % and La/Ni mass ratio = 10 %

silanol groups (Si–OH) in ASEP increases much more than SEP, and the silanol groups (Si–OH) in the SEP are helpful to nickel particles adsorption and dispersion.

The energy dispersive X-ray (EDX) pattern of the K–La–Ni/ASEP is shown in Fig. 2-S. And the signals from Ni, K and La are well attributed to the active component, the signal for Mg, Si, Ca and O are from SEP. EDX analyses of the SEP surface and the prepared catalysts are also shown in Fig. 2-S. Each datum reported is the average value determined from the three locations on the catalyst surface. The results of K, La and Ni loading amount is 0.45, 2.15 and 17.97 wt%.

Fig. 4 shows the XRD patterns of the samples. The crystalline phases and crystallite sizes are depicted in Table 2. It can be seen that only nickel crystalline phases exist in the XRD patterns of the La–Ni/ASEP and K–La–Ni/ASEP catalysts. The characteristic diffraction peaks of nickel in Ni/SEP and Ni/ASEP are more spiculate than those in K–La–Ni/SEP and K–La–Ni/ASEP, it means that there are smaller nickel particles on K–La–Ni trimetallic catalysts. It shows that decoration of potassium and lanthanum is helpful to the nickel particles dispersion, this is also testified by the following hydrogen chemisorption results in Table 3. It is worth noting that the diffraction peaks of nickel in La–Ni/ASEP and K–La–Ni/ASEP are broader than those in Ni/ASEP and it also can be seen from Table 2 that the crystallite sizes of Ni decrease obviously when the lanthanum is added. The results indicate that the doping of lanthanum can evidently decrease the size of the nickel and improve its dispersion. Moreover, it is worth noting that Ni-based/ASEP

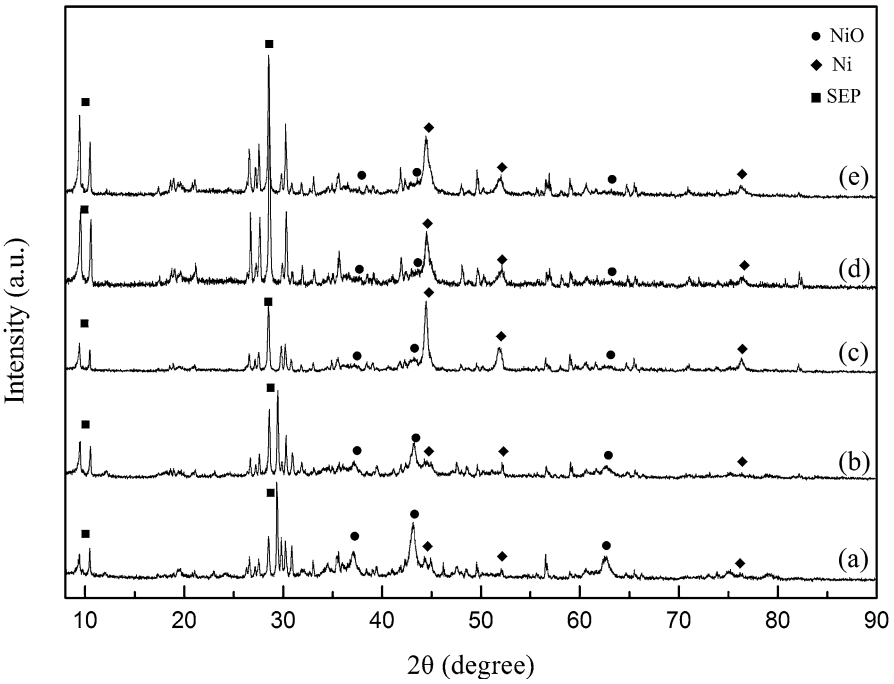

Fig. 4 XRD patterns of different catalysts: Ni/SEP (*a*), K–La–Ni/SEP (*b*), Ni/ASEP (*c*), La–Ni/ASEP (*d*), K–La–Ni/ASEP (*e*). The reduction temperature of the catalysts was 673 K. The K/Ni mass ratio = 2.5 % and La/Ni mass ratio = 10 %

Table 2 XRD identification of different samples

Samples	Crystalline phases	Crystallite sizes of NiO (nm)[a]	Crystallite sizes of Ni (nm)[a]
Ni/SEP[c]	NiO, Ni	25.3	19.8
K–La–Ni/SEP[b,c]	NiO, Ni	12.5	9.1
Ni/ASEP[c]	NiO, Ni	4.5	28.3
La–Ni/ASEP[b,c]	Ni	–	12.1
K–La–Ni/ASEP[b,c]	Ni	–	10.7

[a] Crystallite size estimated from the Scherrer equation

[b] The K/Ni mass ratio = 2.5 % and La/Ni mass ratio = 10 %

[c] The reduction temperature of the catalysts was 673 K

catalysts possesses more Ni metallic phase, which suggests that Ni metallic phase is easier formed from the reduction of Ni^{2+} ions in Ni-based/ASEP. The reason may be the increase in the density of silanol groups (Si–OH) after acid treatment, which is beneficial to nickel particles dispersion and reduction.

Table 3 H_2 chemisorption data of Ni-based series catalysts

Catalysts	H_2 uptake quantity (μL g^{-1})	Metallic surface areas (m^2 g^{-1})	Dispersion (%)
Ni/SEP[b]	14.2	2.9	0.31
K–La–Ni/SEP[a,b]	30.1	4.6	0.86
Ni/ASEP[b]	18.7	4.2	3.1
K–La–Ni/ASEP[a,b]	42.8	7.5	5.3

[a] The K/Ni mass ratio = 2.5 % and La/Ni mass ratio = 10 %

[b] The reduction temperature of the catalysts was 673 K

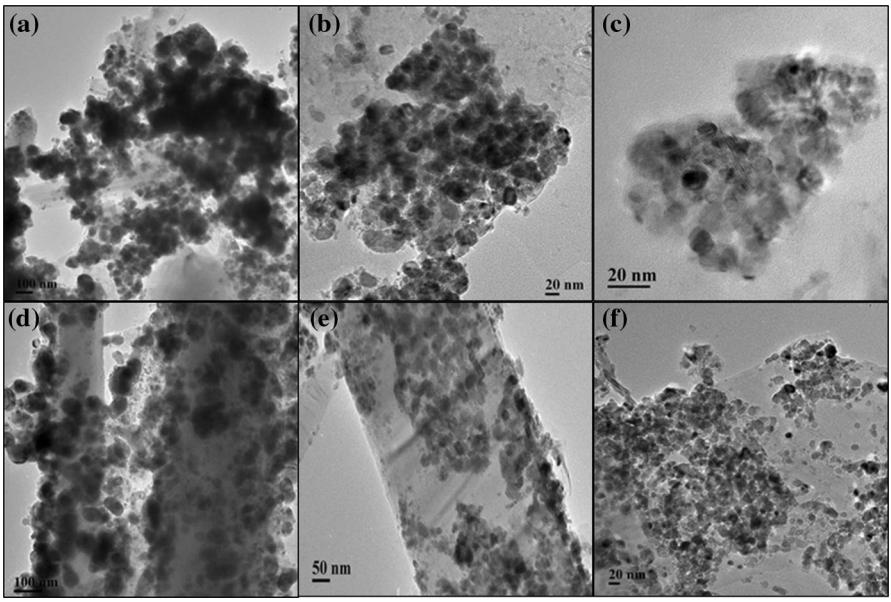

Fig. 5 TEM images of Ni/SEP (**a**), K–La–Ni/SEP (**b**, **c**), Ni/ASEP (**d**), K–La–Ni/ASEP (**e**, **f**). The reduction temperature of the catalysts was 673 K. The K/Ni mass ratio = 2.5 % and La/Ni mass ratio = 10 %

Fig. 5 shows the TEM images of the samples. The dark dots represent the nickel nanoparticles. It can be seen from Fig. 5a that nickel particles agglomerate seriously. However, the nickel particles in K–La–Ni/SEP (Figs. 5b and 5c) and K–La–Ni/ASEP (Figs. 5e and 5f) are more uniformly dispersed on the surface of the catalysts. Moreover, sepiolite supported nickel catalysts modified with potassium and lanthanum possesses smaller nickel nanoparticles of approximately 10 nm.

The H_2 chemisorption data are shown in Table 3. It can be seen that the amount of hydrogen chemisorption is remarkable increasing with the addition of potassium and lanthanum. K–La–Ni/ASEP shows the best nickel dispersion, the largest hydrogen uptake quantity and metallic surface area.

Catalytic performance

The prepared sepiolite supported K–La–Ni trimetallic catalysts were tested in the liquid phase hydrogenation of ADN under the reaction temperature of 363–383 K. In our previous work [29], crystalline Ni–K/α–Al_2O_3 were prepared and used in liquid phase hydrogenation of ADN, it exhibited good performance. However, the loading content of nickel is up to 30 wt% and the reaction temperature is up to 423 K. The results are shown in Table 4. Generally, the conversion of ADN increases and the selectivity to ACN decreases obviously with the increase of the reaction temperatures. Moreover, whether the sepiolite was activated by hydrochloric acid or not, the supported nickel catalysts doped with potassium and lanthanum present higher selectivity to ACN and HMDA. These results suggest that the addition of potassium can effectively inhibit the transamination reactions leading to ACH and C_{12} by-products. It has been demonstrated that potassium, magnesium or other dopant agents have a large impact on the activity and selectivity for nickel based catalysts in ADN hydrogenation [18, 20, 21]. It is worthwhile to note that the existence of potassium inhibit the well-known Thorpe–Ziegler intramolecular condensation of ADN to 2-aminomethylcyclopentylamine (C–C bond formation). It has also been reported that the addition of a certain amount of inorganic base in the reaction medium could improve the selectivity to aminonitrile in the hydrogenation

Table 4 Catalytic properties of Ni-based catalyst for the hydrogenation of ADN under the different reaction temperature

Catalyst	ADN conversion (%)	Temperature (K)	Selectivity (%)			
			ACN	HMDA	ACH	ACN and HMDA
	52.17	363	76.58	4.27	19.15	80.85
Ni/SEP[a,c]	61.26	373	72.16	6.54	21.30	78.70
	72.19	383	68.23	9.55	22.12	77.78
	72.37	363	74.19	9.25	16.56	83.44
K–La–Ni/SEP[a,b,c]	79.21	373	72.15	13.03	14.82	85.18
	87.75	383	70.64	21.52	7.84	92.16
	64.65	363	65.78	12.17	22.05	77.95
Ni/ASEP[a,c]	70.41	373	59.48	15.47	25.05	74.95
	89.44	383	53.22	22.24	24.54	75.46
	84.31	363	67.17	21.58	11.25	88.75
K–La–Ni/ASEP[a,b,c]	90.03	373	63.13	27.09	9.78	90.22
	97.22	383	46.80	35.10	18.10	81.90

[a] *Reaction conditions* stirring rate = 1000 rpm; P_{H2} = 2.0 MPa; Reaction time = 360 min; 50 mL of ethanol; 5 g of ADN; 1 g of Catalyst

[b] The K/Ni mass ratio = 2.5 % and La/Ni mass ratio = 10 %

[c] The reduction temperature of the catalysts was 673 K

of dinitriles over Raney Ni catalysts [7, 23]. The additives of inorganic base could form a stable heterocyclic compound and then interacted with ACN so as to impede its further hydrogenation to 1-amino-6-imino-hexane [11, 13, 14]. Moreover, potassium could also neutralize some acid sites, so as to inhibit the intramolecular condensation of 1-amino-6-imino-hexane to ACH. From the characterization results of XRD (Fig. 4), hydrogen chemisorption (Table 3) and TEM (Fig. 5), we can see that the introduction of potassium and lanthanum decreases the nickel crystal size, improves nickel dispersion and increases the metallic surface area. This may be the reason that potassium and lanthanum doped catalysts show higher activity at the same reaction conditions. It can be seen from the Table 4 that the selectivity to ACN and HMDA is 92.16 % at ADN conversion of 87.75 % over K–La–Ni/SEP, while the selectivity to ACN and HMDA is only 77.78 % at ADN conversion of 72.19 % over Ni/SEP under the same reaction conditions. Similarly, K–La–Ni/ASEP gives 90.22 % selectivity to ACN and HMDA at ADN conversion of 90.03 %, while Ni/ASEP gives 74.95 % selectivity to ACN and HMDA at ADN conversion of 70.41 % under 373 K. Furthermore, compared with sepiolite without acid treatment, acid-activated sepiolite supported nickel monometallic or K–La–Ni trimetallic catalysts present higher catalytic activity under the same reaction conditions. The reason may be the density of silanol groups (Si–OH) can be increased highly by acid treatment and the Si–OH on the surface of sepiolite might aid in nickel adsorption and dispersion. It has been reported that the internal and external surfaces of sepiolite mainly have two kinds of adsorptions sites, one is the –OH coordinated with magnesium ion on the structure edge, and it forms hydrogen bonds, another is the ionic groups of the Si–OH, it will accept a proton or hydrocarbyl compensation remaining electrovalent, and it forms a covalent bond with adsorbate [32–34]. The Si–OH groups may interact with nickel precursor and then form the well-organized and dispersed Si–O–Ni linkages. The Si–O–Ni linkages can be reduced by hydrogen and lead to higher dispersion of nickel particles on the surface of sepiolite. Higher dispersion and larger metallic surface of nickel particles are in favor of hydrogen adsorption and activation, so as to increase the conversion of ADN. This may be the reason that Ni-based/ASEP catalysts possess higher catalytic performance than Ni-based/SEP. Therefore, K–La–Ni/ASEP catalysts present the best catalytic performance, the ADN conversion reaches to 90.03 % under mild reaction conditions of 373 K and 2.0 MPa, the selectivity to ACN and HMDA is up to 90.22 %.

The recycling of the catalysts

The recycling of K–La–Ni/ASEP has been investigated and the results are listed in Table 5. After each reaction, K–La–Ni/ASEP was separated by filtration, dried at room temperature and reduced at 673 K for 4 h. It can be seen from Table 5 that the catalytic activity decreases slightly in the third runs. The inductively coupled plasma atomic emission spectroscopy (ICP-MS) analysis for the third K–La–Ni/ASEP shows that the leaching of the nickel can be neglected. However, the results of XRD patterns and TEM images indicate that nickel particles agglomerate during the regeneration process and this may be the reason that the catalytic activity decreases in the third run.

Table 5 The recycle of K–La–Ni/ASEP in ADN hydrogenation

Run number	ADN conversion (%)	Selectivity (%)			
		ACN	HMDA	ACH	ACN and HMDA
1	89.65	62.57	27.41	10.02	89.98
2	89.44	61.96	26.37	11.67	88.33
3	84.78	56.24	22.81	20.95	79.05

Reaction conditions stirring rate = 1000 rpm; P_{H2} = 2.0 MPa; Reaction time = 360 min; 50 mL of ethanol; 5 g of ADN; 1 g of Catalyst

The K/Ni mass ratio = 2.5 % and La/Ni mass ratio = 10 %

The reduction temperature of the catalysts was 673 K

Conclusions

Sepiolite (SEP) was activated by hydrochloric acid and acid-activated sepiolite (ASEP) supported K–La–Ni trimetallic catalysts were prepared by the incipient impregnation method and characterized by nitrogen adsorption–desorption, temperature programmed reduction (TPR), hydrogen chemisorption, powder X-ray diffraction (XRD), transmission electron microscopy (TEM), scanning electron microscopy (SEM), Fourier transform infrared spectroscopy (FTIR) and energy dispersive X-ray (EDX). The prepared catalysts were tested in the liquid phase hydrogenation of ADN. It was revealed that the potassium could inhibit the formation of the ACH by-product by neutralizing some acid sites on the catalyst, and the introduction of potassium and lanthanum could efficiently reduce the nickel diameter and improve its dispersion. Furthermore, hydrochloric acid treatment increases more silanol groups (Si–OH) on the surface of sepiolite, which is also helpful to nickel particles adsorption and dispersion. The results show that acid activated sepiolite supported K–La–Ni trimetallic catalysts (K–La–Ni/ASEP) present the best catalytic performance, the ADN conversion reaches to 90.03 % under mild reaction conditions of 373 K and 2.0 MPa, the selectivity to ACN and HMDA is up to 90.22 %.

Acknowledgments This work was supported by NSFC (21276218, 21306160), Specialized Research Fund for the Doctoral Program of Higher Education (20124301110007), Project of Hunan Provincial Education Department (14C1093) and Project of Hunan Provincial Science and Technology Department (2015GK1060).

References

1. Yadav GD, Kharkara MR (1995) Appl Catal A 126:115–123
2. Rode CV, Arai M, Shirai M, Nishiyama Y (1997) Appl Catal A 148:405–413
3. Huang Y, Sachtler WMH (1999) Appl Catal A 182:365–378
4. Freidlin LK, Sladkova TA (1964) Russ Chem Rev 33:319
5. Prins R (1997) Catal Today 37:103–120
6. Kajikuri H, Kitamura M, Higashio Y (1994) US Patent 5304643A

7. Fischer R, Bassler P, Luyken H, Ohlbach F, Melder JP, Merger M, Ansmann A, Rehfinger A, Voit G (2002) US Patent 6359178B1
8. Bassler P, Luyken H, Achhammer G (1998) US Patent 5717090A
9. Sheldon R (2000) Green Chem 2:G1–G4
10. Serra M (2002) J Catal 209:202–209
11. Serra M, Salagre P, Cesteros Y, Medina F, Sueiras JE (2000) Solid State Ion 134:229–239
12. Alini S, Bottino A, Capannelli G, Comite A, Paganelli S (2005) Appl Catal A 292:105–112
13. Serra M, Salagre P, Cesteros Y, Medina F, Sueiras JE (2004) Appl Catal A 272:353–362
14. Tichit D, Durand R, Rolland A, Coq B, Lopez J, Marion P (2002) J Catal 211:511–520
15. Zhao L, Wang CY, Chen JX, Zhang JY (2007) Chin Chem Lett 18:685–688
16. Yu XB, Li HX, Deng JF (2000) Appl Catal A 199:191–198
17. Li H, Xu Y, Li H, Deng JF (2001) Appl Catal A 216:51–58
18. Medina F, Salagre P, Sueiras JE, Fierro JLG (1993) Solid State Ion 59:205–210
19. Medina F, Salagre P, Sueiras JE, Fierro JLG (1993) J Chem Soc Faraday Trans 89:3507–3512
20. Medina F, Salagre P, Sueiras JE, Fierro JLG (1993) J Mol Catal 81:387–395
21. Medina F, Salagre P, Sueiras JE, Fierro JLG (1993) J Chem Soc Faraday Trans 89:3981–3986
22. Medina F, Salagre P, Sueiras JE, Fierro JLG (1993) Appl Catal A 99:115–129
23. Cotting MC, Gilbert L, Leconte P (1999) US Patent 5981790A
24. Ziemecki SB (1992) US Patent 5151543A
25. Mark H (2000) WO Patent 00/27526A1
26. Beatty RP, Paciello RA (1996) US Patent 5554778A
27. Beatty RP, Paciello RA (1996) US Patent 5559262A
28. Beatty RP, Paciello RA (1997) US Patent 5599962A
29. Liao HG, Liu SH, Hao F, Liu PL, You KY, Liu DD (2013) Luo Ha. React Kinet Mech Cat 109:475–488
30. Anderson JA, Falconer SE, Galán-Fereres M (1997) Spectrochim Acta A 53:2627–2639
31. Núñez K, Gallego R, Pastor JM, Merino JC (2014) Appl Clay Sci 101:73–81
32. Valentín JL, López-Manchado MA, Posadas P, Rodríguez A, Marcos-Fernández A, Ibarra L (2006) J Colloid Interface Sci 298:794–804
33. Sabah E, Majdan M (2009) J Food Eng 91:423–427
34. Sabah E (2007) J Colloid Interface Sci 310:1–7
35. Esteban-Cubillo A, Pina-Zapardiel R, Moya JS, Barba MF, Pecharromán C (2008) J Eur Ceram Soc 28:1763–1768
36. Sabah E, Turan M, Çelik MS (2002) Water Res 36:3957–3964
37. Damyanova S, Daza L, Fierro JLG (1996) J Catal 159:150–161
38. Zhu Q, Zhang Y, Lv F, Chu PK, Ye Z, Zhou F (2012) J Hazard Mater 217:11–18
39. Shoval S, Michaelian KH, Boudeulle M, Panczer G, Lapides I, Yariv S (2002) J Therm Anal Calorim 69:205–225
40. Zotov N, Keppler H (2002) Chem Geol 184:71–82
41. Zhang M, Shi L, Yuan S, Zhao Y, Fang J (2009) J Colloid Interface Sci 330:113–118